A kinetic two-scale damage model for high-cycle fatigue simulation using multi-temporal Latin framework

Mainak Bhattacharyya, Amélie Fau, Rodrigue Desmorat, Shadi Alameddin, David Néron, Pierre Ladevèze, Udo Nackenhorst

A kinetic two-scale damage model for high-cycle fatigue simulation using multi-temporal Latin framework

Mainak Bhattacharyya[a,*], Amélie Fau[b], Rodrigue Desmorat[c], Shadi Alameddin[b], David Néron[c], Pierre Ladevèze[c], Udo Nackenhorst[b]

[a] LaMCoS, INSA-Lyon, CNRS UMR 5259, Université de Lyon, Bâtiment Sophie Germain, 27 bis avenue Jean Capelle, 69621 Villeurbanne Cedex, France
[b] IBNM, Leibniz Universität Hannover, Appelstraße 9a, 30167 Hannover, Germany
[c] LMT, ENS Paris-Saclay, CNRS, Université Paris Saclay, 61 avenue du Président Wilson, 94235 Cachan Cedex, France

The goal of this paper is to introduce a model order reduction method for high-cycle fatigue simulations using a kinetic damage model, i.e. a constitutive model in which the damage evolution law is defined as a rate form $\dot{D} = \frac{\mathrm{d}}{\mathrm{d}t}D$ for the damage variable D. In the framework of continuum mechanics, high-cycle fatigue simulation involves a two-scale damage model, which includes macroscopic elastic and microscopic plastic behaviours, for a very large number of cycles. Unlike the classical usage of the two-scale damage model by Lemaitre and co-workers, where damage is calculated as a post-process of an elastic or elasto-plastic macroscopic analysis, in this work, a fully coupled analysis is conducted assuming a macroscopic damage feedback from its microscopic counterpart. Damage is considered to be isotropic with micro-defect closure effect on both macroscopic and microscopic scales. To overcome the numerical expense, the large time increment (LATIN) method is used as a linearisation framework, where the constitutive behaviour is separated from the global admissibility which in turn is solved through separation of variables using a proper generalised decomposition (PGD)-based model reduction method. A multi-temporal discretisation approach is henceforth used based on finite element like description in time for the quantities of interest, providing a sophisticated numerical approach suitable for high-cycle fatigue simulation under complex loading.

1. Introduction

High-Cycle Fatigue (HCF) is one of the major reasons behind the failure of engineering structures. In metals, it is governed by macro-elasticity and micro-plasticity (plasticity at the defects scale) and the load carrying capacity is progressively decreased with successive load fluctuations. For HCF to occur, the loading should cause stress levels at the macro-scale below the yield stress, so that the macroscopic behaviour of the material remains elastic. However, plasticity and damage may occur at the micro-scale (see Lemaitre, 1996; Dang Van, 1999; Lemaitre and Desmorat, 2005). The simulations of HCF processes are hindered not only by the requirement of sophisticated multi-scale models, deterministic (Lemaitre and Doghri, 1994a; Lemaitre et al., 1999; Desmorat et al., 2007; Lautrou et al., 2009; Gaborit, 2015; Gaborit et al., 2016) or probabilistic (Doudard et al., 2005), but also by the need of sophisticated numerical techniques such that a large number of cycles can be simulated.

An energy-based micro-crack propagation theory has been used to describe damage evolution at the macro-scale through homogenisation Dascalu (2009). In Monchiet et al. (2006), a two-scale model describing the physical micromechanism at the grain scale has been proposed. The presence of persistent slip systems leads to the presence of plasticity at the grain scale, eventhough the loading is below the macroscopic fatigue limit. With the same interest of providing models for high cycle fatigue based on microdeformation mechanics, HCF simulation based on representative volume elements of the microstructure has been introduced in Gillner and Münstermann (2017).

In the framework of continuum damage mechanics (CDM), which is a branch of the classical continuum mechanics, the loss of load-bearing capacity is described through a dedicated internal variable in a thermodynamically consistent framework (see Besson et al., 2010). The most classical usage of CDM for the description of HCF with proper agreement with experimental data was in Chaboche and Lesne (1988); Xiao et al. (1998). Thereafter, damage evolution based on endurance surface was presented in Ottosen et al. (2008). In this context and for HCF, a two-scale damage model was proposed in Lemaitre and Doghri

* Corresponding author.
E-mail address: mainak.bhattacharyya@insa-lyon.fr (M. Bhattacharyya).

(1994b); Lemaitre et al. (1999) based on the idea that in HCF the macroscopic elastic behaviour is maintained while at the microscopic scale, micro-cracks/micro-voids are initiated and developed without affecting the macroscopic elastic behaviour. Such behaviours are simulated using an elastic finite element structural computation at the macro-scale and a post-processing analysis of the micro-damage evolution at the critical stress points. The failure of the corresponding representative volume element (RVE) at the meso-scale occurs when the microscopic damage reaches the critical value (see Lemaitre, 1996). This kind of uncoupled analysis seems unrealistic as the macroscopic behaviour is assumed to be bereft of damage; however, failure still occurs. Therefore, a more realistic approach would be to have a damage description on the macro-scale, influenced by its counterpart at the micro-scale. This issue is addressed, in the current work, by introducing a backward coupling of the damage variable from the micro-scale to the macro-scale. A recent work (see Tang et al., 2017), modified the classical version of the two scale damage model to model the high to low cycle fatigue transition using a novel two-scale representative volume element.

One of the key components when constructing damage models for cyclic loading is the so-called quasi-unilateral condition of micro-defect closure effect (see Lemaitre and Desmorat, 2005). This idea translates into different damage evolution rates in tension and in compression. The first usage of this methodology was in Ladevèze and Lemaitre (1984), where a closure parameter to quantify the difference between tensile and compressive behaviours was introduced. This model has been extended later to include anisotropic damage variable (see Desmorat and Cantournet, 2008). However, in order to ensure convexity of the yield surface in this work, the quasi-unilateral effect is introduced only on the hydrostatic stress (see Desmorat and Cantournet, 2008).

Damage mechanics, although replicates the physical phenomena in a thermodynamically consistent manner, can be numerically expensive, especially for fully coupled analysis (see Desmorat et al., 2007) and probably infeasible for real engineering structures. This issue becomes more predominant for structural pre-design where quick methods are required to predict the life-time of a structure and its possible failures. A fast identification of localised plasticity and damage based on an energetic approach Desmorat (2002), developed after the historical works of Neuber (1961) and Glinka (1985), can be a solution. On the other hand, model order reduction (MOR) techniques can make such computations feasible and efficient. For instance, an adaptive proper orthogonal decomposition with a local/global sub-domains technique was used in Kerfriden et al. (2011, 2012) to reduce the computational effort associated with damage computations. Another adaptive MOR technique was introduced by Ryckelynck et al. (2011), where based on a priori hyper-reduction approach, the subspace spanned by the MOR shape functions is extended and at the same time the quantities of interest are integrated over a reduced integration domain. Proper generalised decomposition (PGD) is also a priori model reduction technique that reduces the problem's dimensionality to circumvent the numerical expense, as done in Allix et al. (1989) for plasticity-based damage models and in Bhattacharyya et al. (2018a) for viscoplasticity-based damage models, in the context of the large time increment (LATIN) method.

LATIN method, introduced first in Ladevèze (1985a, b), is a robust strategy to address history-dependent non-linearities. It separates the local and non-linear material behaviour from the global linearised equilibrium, in which a space-time separated representation induces spectacular efficiency and time saving (see Ladevèze, 1999, for details). LATIN has been used extensively over the years with appreciable performance for material non-linearities especially for visco-plasticity (see Ladevèze et al., 2010; Relun et al., 2013, for instance), unilateral contact (see Giacoma et al., 2015), or parametric studies (see Heyberger et al., 2011; Néron et al., 2015).

For fatigue simulation, the numerical challenge is particularly due to the large number of cycles involved in the computation. A traditional method to overcome this cost is jump cycles (see Lemaitre and Doghri, 1994b; Van Paepegem et al., 2001). In this method, instead of a cycle-by-cycle simulation, full blocks of cycles are skipped and only certain cycles are computed. From the information of a particular simulated cycle, the tendency of the quantities of interest and the number of cycles to be jumped over are extrapolated and estimated respectively. These jumps along with the corresponding extrapolations continue till the complete temporal domain is encompassed or the critical damage value is reached (see Lemaitre and Desmorat, 2005). Another jump cycle method was proposed in Burlon et al. (2014). For combined cyclic fatigue, a temporal homogenisation technique was investigated by several authors (Devulder et al., 2010; Haouala and Doghri, 2015). This homogenisation results in a number of initial boundary value problems on different time scales. A different strategy to tackle HCF computations is extended finite element method based on enrichment functions in time, which have the temporal characteristic of the loading (see Bhamare et al., 2014). An alternate fully-discrete approach is the multi-temporal model order reduction method that has been proposed for cyclic plasticity (see Cognard and Ladevèze, 1993) and recently extended for fatigue damage computation (see Bhattacharyya et al., 2018c). This approach is based on a finite element like time discretisation, where each time element is confined within two successive cycles, termed as nodal cycles, and only these cycles are computed then the solution is interpolated over the time element. This idea can be interpreted as a variant of the classical jump cycle algorithm with temporal interpolation. The adaptive multi-temporal scale discretisation has proved efficient in Bhattacharyya et al. (2018c, b) for different academic examples in low-cycle fatigue regime using a macro-scale viscoplasticity-based damage model.

The goal of this contribution is to extend the multi-scale LATIN-PGD framework to tackle high-cycle fatigue computations, involving a fully coupled quasi-brittle damage model. This is one of the first attempts to solve the two-scale damage formulation in a non-incremental framework. Contrary to the classical uncoupled formulation of the two-scale damage model which is based on post-processing of structural calculations, a two-way coupling behaviour is used to achieve better physical representation. This approach of providing a damage feedback to the macro-scale is also novel in its own right. The solution of the global admissibility condition is performed through Galerkin-based PGD formulations for both spatial and temporal problems. For the temporal quantities of interest a finite element like description is used involving the computation of only certain cycles and interpolating the quantities of interest over the rest of the cycles.

The article is structured as follows. In section 2, the continuum damage theory along with the used two-scale damage model are introduced. In section 3, the innovative algorithm based on multi-temporal LATIN-PGD model order reduction technique is detailed. Finally, in section 4, the algorithm is tested on different academic examples.

2. Two-scale damage model

The problem of interest is a continuous structure under a quasi-static and isothermal loading defined over time domain $[0, T]$. The body can be subjected to body forces f_d on its domain Ω, as illustrated on Fig. 1. A part $\partial_1\Omega$ of the boundary $\partial\Omega$ may be subjected to prescribed displacements u_d, and traction forces F_d may be prescribed on the complementary part of the boundary $\partial_2\Omega$. The state of such structure is defined by thermodynamically consistent state variables, observable or internal ones. These variables not only satisfy the local material behaviour (constitutive laws) but also must satisfy the global admissibility conditions (equilibrium equation).

In the framework of continuum damage mechanics, a variant of the two-scale damage model proposed in Lemaitre (1996) is considered here. The underlying concept of this sophisticated damage model in the context of high-cycle fatigue is to have the macroscopic material

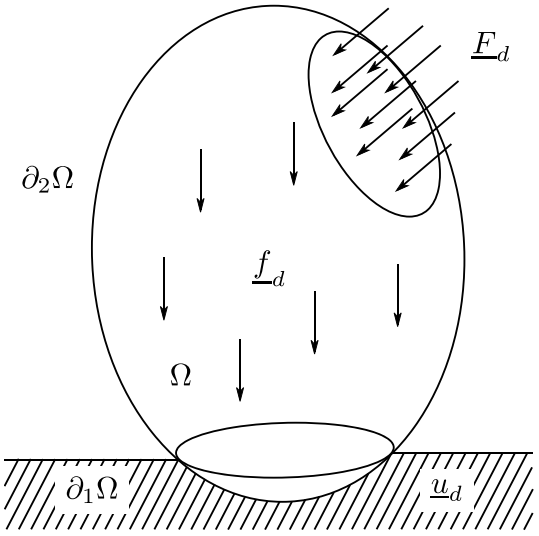

Fig. 1. Reference problem in domain Ω.

behaviour purely elastic, but non-linear due to the presence of macroscopic damage which arises because of the damage existence at the micro-scale which in turn is governed by micro-plasticity.

A key point of present work is that fatigue damage is considered as part of the material behaviour, i.e. as part of the constitutive equations, in a so-called kinetic damage model: the damage evolution law is written in rate form $\dot{D} = \frac{\mathrm{d}D}{\mathrm{d}t} = \cdots$ for the damage variable D.

2.1. Macro-scale: elastic behaviour with unilateral damage

The admissibilities of the state variables at the macro-scale are defined by the equilibrium equation, which in its weak form reads

$$\int_{[0,T]\times\Omega} \boldsymbol{\sigma}\colon \boldsymbol{\varepsilon}(\underline{u}^*)\,\mathrm{d}\Omega\,\mathrm{d}t = \int_{[0,T]\times\Omega} \underline{f}_d\cdot\underline{u}^*\mathrm{d}\Omega\,\mathrm{d}t + \int_{[0,T]\times\partial_2\Omega} \underline{F}_d\cdot\underline{u}^*\,\mathrm{d}S\,\mathrm{d}t, \quad \forall\ \underline{u}^* \in \mathcal{U}^0, \tag{1}$$

where $\mathcal{U}^0$ is the space associated with the kinematically admissible field $\underline{u}$ and the stress tensor $\boldsymbol{\sigma}$ is statically admissible. From the displacement field $\underline{u}$, the kinematically admissible infinitesimal total strain tensor $\boldsymbol{\varepsilon}$ is defined as

$$\boldsymbol{\varepsilon} = \frac{1}{2}(\nabla\underline{u} + (\nabla\underline{u})^T). \tag{2}$$

For HCF loading, governed by macro-elasticity, the total strain tensor only comprises of the elastic contribution $\boldsymbol{\varepsilon}^e$ as the plastic contribution $\boldsymbol{\varepsilon}^p$ vanishes (see Lemaitre et al., 1999).

Considering isotropic damage, defined by a scalar variable D, the prescribed cyclic loading induces the phenomenon of micro-defects closure (see Lemaitre, 1996; Lemaitre and Desmorat, 2005). The importance of that phenomenon is generally evaluated through a closure parameter, the value of which lies between 0 corresponding to complete stiffness recovery, and 1 corresponding to no stiffness recovery. However, closure is introduced here only with respect to the hydrostatic part of the stress and the deviatoric part is assumed to be bereft of any closure effect, i.e. the yield surface is not affected by the closure. This provides an alternative definition of the effective stress as

$$\tilde{\boldsymbol{\sigma}} = \frac{\boldsymbol{\sigma}_D}{1-D} + \left[\frac{\langle\sigma_H\rangle}{1-D} - \langle -\sigma_H\rangle\right]\mathbb{I}, \tag{3}$$

such that the non-linear elastic state law becomes

$$\tilde{\boldsymbol{\sigma}} = \mathbf{C}\boldsymbol{\varepsilon}, \tag{4}$$

where $\mathbf{C}$ is the classical elasticity tensor defined using the modulus of elasticity E and the Poisson ratio ν. The deviatoric stress is represented by $\boldsymbol{\sigma}_D = \boldsymbol{\sigma} - \sigma_H\mathbb{I}$, and $\sigma_H = \frac{1}{3}\mathrm{tr}\boldsymbol{\sigma}$ is the hydrostatic part. The Macaulay brackets $\langle\bullet\rangle$ denote the positive part of the considered quantity $\bullet$, and $\mathbb{I}$ is the identity matrix.

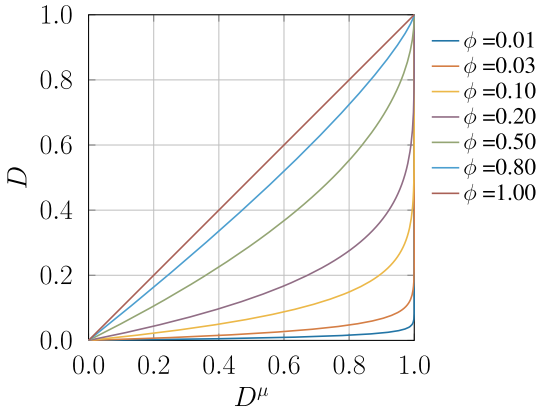

Fig. 2. Effect of the micro-damage evolution on the macro-damage for different values of the parameter φ(from Gaborit, 2015).

Unlike the previous versions of the two-scale model, a coupling effect between the damage values at the two length scales is introduced, which basically translates into the following relationship (see Gaborit et al., 2016),

$$D = 1 - (1 - D^\mu)^\varphi, \tag{5}$$

where D^μ denotes the damage at the micro-scale and the parameter φ dictates the degree of coupling between the two length scales, with $\varphi = 1$ providing the strongest possible coupling ($D = D^\mu$) and $\varphi = 0$ induces no coupling at all () (see Gaborit et al., 2013; Gaborit, 2015). On Fig. 2 the effect of the micro-damage on the macro-damage, which has been extensively investigated in Gaborit (2015), can be observed for different values of the parameter φ. The idea of using such coupling term is to mimic the HCF failure, where the macroscopic damage retains a very low value for most of the structural lifetime and shows a drastic increase towards the end, i.e. towards reaching the critical damage D_c corresponding to the failure of the material due to the initiation of macro-cracks. Lower the value of φ is, longer the macro-damage remains to a small value whereas the micro-damage increases. Therefore, the HCF damage phenomenon can be captured using low values of φ.

2.2. Micro-scale: coupled elasto-plastic-damage behaviour

In the current model, the defects at the micro-scale are represented by a weak inclusion subjected to plasticity and damage in a meso-scale representative volume element (RVE) as shown in Fig. 3 (Lemaitre and Doghri, 1994b). The matrix part of the RVE, which is endowed with the RVE macro-scale effective material properties, remains elastic but coupled with macroscopic damage resulting from its microscopic counterpart (Besson et al., 2010). The idea is that the RVE effective behaviour is representative of that of the material as a whole. Thus, each Gauss point is associated with an RVE, which is chosen such that the heterogeneous nature of the material is statistically well represented, i.e. the dimension of the micro-defect l_μ is much smaller than the meso-scale size l_{RVE}, which is itself much smaller than the characteristic length of the structure l_M. Hereafter, the mechanical properties of the material of interest at the micro-scale, i.e. in the microscopic inclusion, are detailed. They are described in a general framework by a set of constitutive relations including plasticity, damage and kinematic hardening (see Lemaitre and Desmorat, 2005).

The total micro-strain tensor $\boldsymbol{\varepsilon}^\mu$ can be additively decomposed into an elastic contribution $\boldsymbol{\varepsilon}^{\mu,e}$ and a plastic contribution $\boldsymbol{\varepsilon}^{\mu,p}$. To maintain

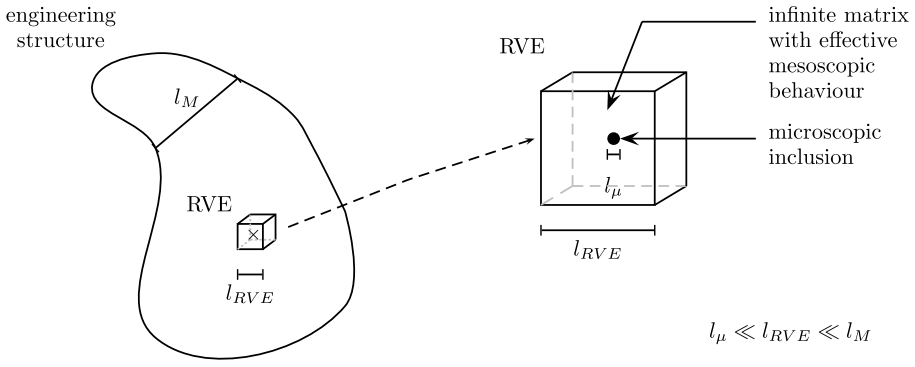

Fig. 3. Schematic representation of the RVE for the two-scale damage model.

the convexity properties, considering unilateral damage, the effective stress at that scale $\tilde{\boldsymbol{\sigma}}^\mu$ is defined, similar to that of the macro-scale, by its hydrostatic part $\sigma_H^\mu \mathbb{I}$ and the deviatoric one $\boldsymbol{s}_D^\mu$. The compressive contribution of the hydrostatic part has a full recovery, whereas the tensile part of the hydrostatic stress has no recovery at all, i.e.

$$\tilde{\boldsymbol{\sigma}}^\mu = \frac{\boldsymbol{s}_D^\mu}{1-D^\mu} + \left[\frac{\langle \sigma_H^\mu \rangle}{1-D^\mu} - \langle -\sigma_H^\mu \rangle\right]\mathbb{I}. \tag{6}$$

The equations of state for the elasto-plastic materials read

$$\tilde{\boldsymbol{\sigma}}^\mu = \mathbf{C}\boldsymbol{\varepsilon}^{\mu,e}, \tag{7a}$$

$$Y^\mu = R_v \frac{(\tilde{\sigma}_{eq}^\mu)^2}{2E}, \tag{7b}$$

$$\boldsymbol{\beta}^\mu = \mathbf{Q}\boldsymbol{\alpha}^\mu. \tag{7c}$$

Similar to the macro-scale, the non-linear elastic state law incorporating damage is given by eq. (7a). The thermodynamic force corresponding to the micro-scale damage is the strain energy release rate Y^μ defined in eq. (7b), which is non-linear with respect to the damage variable and the stress tensor. The effects due to the direction of the loading are described through the triaxiality function R_v, which is defined as

$$R_v = \frac{2}{3}(1+\nu) + 3(1-2\nu)\langle \frac{\sigma_H^\mu}{\sigma_{eq}^\mu} \rangle^2, \tag{8}$$

with $\sigma_H^\mu = \frac{1}{3}(\mathrm{tr}\boldsymbol{\sigma}^\mu)$ being the hydrostatic part of the stress tensor, $\sigma_{eq}^\mu = \sqrt{\frac{3}{2}\sigma_{D_{ij}}^\mu \sigma_{D_{ij}}^\mu}$ and $\tilde{\sigma}_{eq}^\mu = \sqrt{\frac{3}{2}\tilde{\sigma}_{D_{ij}}^\mu \tilde{\sigma}_{D_{ij}}^\mu}$ being the equivalent stress and the equivalent of the effective stress at the micro-scale, respectively. The relationships between the internal variables describing the kinematic hardening of the material i.e. $\boldsymbol{\alpha}^\mu$ and their corresponding thermodynamic forces $\boldsymbol{\beta}^\mu$ are given by eq. (7c) through the tensor $\mathbf{Q}$ which incorporates the kinematic hardening modulus Q. The evolution equations for plasticity, hardening and damage at the micro-scale are given by

$$\dot{\boldsymbol{\varepsilon}}^{\mu,p} = \frac{3}{2}\frac{\tilde{\boldsymbol{\sigma}}^\mu - \boldsymbol{\beta}^\mu}{(\tilde{\boldsymbol{\sigma}}^\mu - \boldsymbol{\beta}^\mu)_{eq}}\frac{\dot{\lambda}_p}{1-D^\mu}, \tag{9a}$$

$$\dot{\boldsymbol{\alpha}}^\mu = \frac{3}{2}\frac{\tilde{\boldsymbol{\sigma}}^\mu - \boldsymbol{\beta}^\mu}{(\tilde{\boldsymbol{\sigma}}^\mu - \boldsymbol{\beta}^\mu)_{eq}}\dot{\lambda}_p, \tag{9b}$$

$$\dot{D}^\mu = \left(\frac{Y^\mu}{S}\right)^s \dot{p}^\mu, \ \text{if } p^\mu > p_D. \tag{9c}$$

The evolution of the plastic strain with respect to time is given by eq. (9a), where $\dot{\lambda}_p$ is the plastic multiplier obtained from the consistency condition with the micro-scale yield function f^μ given as

$$f^\mu = (\tilde{\sigma}_D^\mu - \boldsymbol{\beta}^\mu)_{eq} - \sigma_f^\infty, \tag{10}$$

with $\tilde{\boldsymbol{\sigma}}_D^\mu$ being the deviatoric part of the effective stress and the asymptotic fatigue limit σ_f^∞ considered as the micro-scale yield stress. Therefore, for any stress level below the asymptotic fatigue limit, neither micro-plasticity nor damage is induced, and the structure can survive an infinite number of cycles (see Lemaitre and Desmorat, 2005). Loading-unloading criterion is given by the classical Kuhn-Tucker condition

$$\dot{\lambda}_p \geq 0, \ f^\mu \leq 0, \ \dot{\lambda}_p f^\mu = 0. \tag{11}$$

The evolution of the kinematic hardening internal variable is similar to that of the plastic strain excluding damage and it is described by eq. (9b). The cumulative plastic strain, defined in rate form as

$$\dot{p}^\mu = \left(\frac{2}{3}\dot{\boldsymbol{\varepsilon}}^{\mu,p} : \dot{\boldsymbol{\varepsilon}}^{\mu,p}\right)^{1/2}, \tag{12}$$

is related to the plastic multiplier and the damage variable through

$$\dot{p}^\mu = \frac{\dot{\lambda}_p}{1-D^\mu}. \tag{13}$$

Along with the material parameters S and s, the evolution of damage is also governed by $\dot{p}^\mu$ according to eq. (9c) and the threshold p_D is considered here to be zero.

2.3. Scale transition based on the self-consistent scheme

The macro-micro scale transition is based on the assumption that the RVE comprises of a spherical isotropic inclusion in an infinite isotropic homogeneous matrix with effective mechanical properties (see Kröner, 1961; Zaoui, 1985; Berveiller and Zaoui, 1979). Thus, knowing the deformation at the macro-scale, the total deformation and the plastic deformation at the micro-scale are defined using the Eshelby-Kröner localisation law (see Eshelby, 1957; Besson et al., 2010) for non-linear behaviours as

$$(\boldsymbol{\varepsilon}^\mu - \boldsymbol{\varepsilon}) = \gamma(\boldsymbol{\varepsilon}^{\mu,p} - \boldsymbol{\varepsilon}^p), \tag{14}$$

where γ is the Eshelby coefficient given by

$$\gamma = \frac{2}{15}\frac{4-5\nu}{1-\nu}, \tag{15}$$

and the plastic deformation at the macro-scale $\boldsymbol{\varepsilon}^p$ vanishes due to the elasticity assumption.

As summarised in Fig. 4, it has to be mentioned that the macroscopic quantities of interest should satisfy the global admissibility condition defined by eq. (1) along with the macroscopic material behaviour, however, the micro quantities of interest need to satisfy only the microscopic material behaviour.

2.4. Multi-temporal Latin approach

Instead of using classical time incremental methods to solve non-linear problems, a non-incremental approach, i.e. the LATIN method is

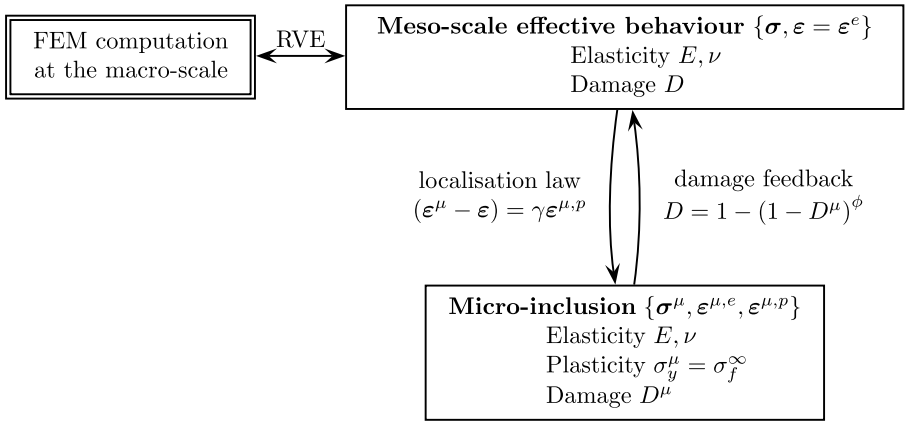

Fig. 4. Schematic representation of the finite-element computation using the two-scale damage model.

used as a solution framework in this research. It starts with an initialisation for the quantities of interest over the complete space-time domain and then successive corrections are added to the initial guess till convergence is reached. The utility of the LATIN method lies on the fact that the governing equations are separately solved, i.e. for a given instant only the local material behavioural laws are solved and for the next instant the linearised form of the equilibrium equation is solved.

For the given context of fatigue damage simulation involving large number of cycles, LATIN method when employed for the complete temporal domain may render the simulation extremely expensive. Hence an innovative scheme is used which basically segregates the complete time domain into separate time elements which are demarcated by nodal cycles. LATIN method thereafter is used to calculate the quantities of interest at the nodal cycles and the intermediate cycles can then be interpolated using temporal shape functions. This approach can be viewed as a modified, non-incremental version of the classical jump-cycle algorithm.

This idea boils down to two separated temporal discretisations of the quantities of interest as illustrated in Fig. 5:

- a coarse scale discretisation θ which represents the slow evolution of the quantities of interest along the cycles, chosen to be the initial time point of every cycle,
- a fine scale discretisation τ at each cycle representing the fast evolution of the quantities of interest within the cycle.

The continuous time field t may then be approximated using the two-scale discretisation as

$$t = \theta_i + \tau_i, \text{ with } i \in [0, N-1] \text{ and } \tau_i \in [0, \Delta T], \tag{16}$$

with N being the total number of cycles comprised in the temporal domain and ΔT being the time period.

As emphasised before, the nodal cycles are calculated using the LATIN algorithm on the fine scale τ, the knowledge of which is used then to evaluate the quantities of interest on the whole time element through interpolation on the coarse scale θ.

2.5. Computation of one nodal cycle of interest

For a given nodal cycle m, the solution set is initialised from the converged solution of the previous nodal cycle $m-1$. In the case of the first nodal cycle (i.e. $m = 0$) the initialisation is obtained from a linear elastic solution considering all the boundary conditions. After the initialisation, non-linear corrections are added at each iteration till convergence is reached.

The separation of difficulties in LATIN introduces two separate manifolds, one corresponding to the space of local constitutive behaviour, and the other corresponding to the global admissibility conditions. From a given solution $\boldsymbol{s}_i$ belonging to the global manifold $\boldsymbol{A_d}$, the idea is first to seek the solution set $\hat{\boldsymbol{s}}_{i+1/2}$ belonging to the non-linear manifold $\boldsymbol{\Gamma}$ through the computation of $\boldsymbol{s}^\mu$, which is the solution set at

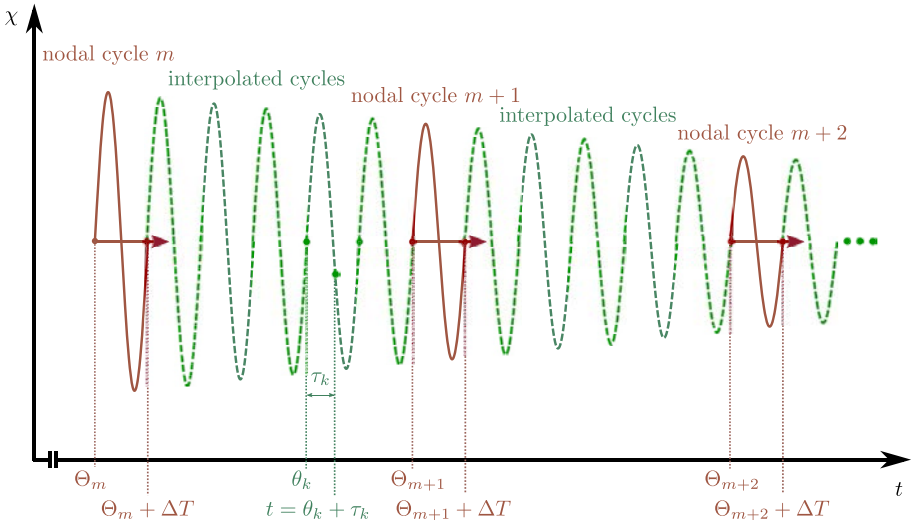

Fig. 5. Two temporal scale discretisations.

the micro-scale. It must be noticed that $\hat{\boldsymbol{s}}_{i+1/2}$ and $\boldsymbol{s}^{\mu}$ are obtained through the solution of the scale transition equation given by eq. (14), the constitutive relations at both length scales, i.e. eqs. (4), (7) and (9) and the coupled damage equations, i.e. eq. (5). Thereafter, knowing $\hat{\boldsymbol{s}}_{i+1/2}$, the solution set $\boldsymbol{s}_{i+1}$ is calculated by solving the global equilibrium equation defined by eq. (1). The macroscopic quantities of interest must be calculated such that $\boldsymbol{s} \in \boldsymbol{A_d}$ and $\hat{\boldsymbol{s}} \in \boldsymbol{\Gamma}$, however, their microscopic counterparts only satisfy the microscopic local equations. To be more simplistic, the primary quantities of interest are the macroscopic quantities, the exact solution of which lies in the intersection of $\boldsymbol{A_d}$ and Γ, and the microscopic quantities of interest are just intermediaries to obtain $\hat{\boldsymbol{s}}$ in the local stage.

2.5.1. Latin local stage

Knowing $\boldsymbol{s}_i$, the first stage of each iteration looks for the solution $\hat{\boldsymbol{s}}_{i+1/2}$ in the space $\boldsymbol{\Gamma}$, which also involves the calculation of the solution set $\boldsymbol{s}^{\mu}$. The transfer of information from the global to the local stage occurs through the search direction equation given by

$$(\hat{\boldsymbol{\varepsilon}}_{i+1/2} - \boldsymbol{\varepsilon}_i) + \mathbf{H}^{+}(\hat{\boldsymbol{\sigma}}_{i+1/2} - \boldsymbol{\sigma}_i) = 0. \tag{17}$$

Following Ladevèze (1999), for the direction of ascent, the search direction operator is assumed such that $(\mathbf{H}^{+})^{-1} = 0$, which gives $\hat{\boldsymbol{\sigma}}_{i+1/2} = \boldsymbol{\sigma}_i$. It should be noted that the search direction operator mainly influence the rate of convergence and not the converged solution.

At a current time step j the macroscopic strain is calculated from the macroscopic effective stress through

$$\hat{\boldsymbol{\varepsilon}}_j = \boldsymbol{C}^{-1}\hat{\boldsymbol{\sigma}}_j, \tag{18}$$

where the effective stress is given by

$$\hat{\boldsymbol{\sigma}}_j = \boldsymbol{\sigma}_{D,j} + \left[\frac{\langle \sigma_{H,j} \rangle}{1 - \hat{D}_{j-1}} - \langle -\sigma_{H,j} \rangle\right]\mathbb{I}. \tag{19}$$

Knowing the strain state at the macro-scale, the micro-strain is elastically initialised through the localisation law and the rest of the quantities of interest are initialised from the previous time step. The trial state is thereby defined as

$$\boldsymbol{\varepsilon}_j^{\mu,e^{\text{trial}}} = \boldsymbol{\varepsilon}_{j-1}^{\mu,e} + (\hat{\boldsymbol{\varepsilon}}_j - \hat{\boldsymbol{\varepsilon}}_{j-1}), \tag{20a}$$

$$\boldsymbol{\varepsilon}_j^{\mu,p^{\text{trial}}} = \boldsymbol{\varepsilon}_{j-1}^{\mu,p}, \tag{20b}$$

$$p_j^{\mu^{\text{trial}}} = p_{j-1}^{\mu}, \tag{20c}$$

$$\boldsymbol{\alpha}_j^{\mu^{\text{trial}}} = \boldsymbol{\alpha}_{j-1}^{\mu}, \tag{20d}$$

$$\boldsymbol{\beta}_j^{\mu^{\text{trial}}} = \boldsymbol{\beta}_{j-1}^{\mu}, \tag{20e}$$

$$D_j^{\mu^{\text{trial}}} = D_{j-1}^{\mu}. \tag{20f}$$

Then, the trial stress state $\boldsymbol{\sigma}_j^{\mu^{\text{trial}}}$ is evaluated from the non-linear elastic state law as

$$\tilde{\boldsymbol{\sigma}}_j^{\mu^{\text{trial}}} = \mathbf{C}\boldsymbol{\varepsilon}_j^{\mu,e^{\text{trial}}}, \tag{21}$$

with

$$\tilde{\boldsymbol{\sigma}}_j^{\mu^{\text{trial}}} = \frac{\boldsymbol{\sigma}_{D,j}^{\mu^{\text{trial}}}}{1 - D_j^{\mu^{\text{trial}}}} + \left[\frac{\langle \sigma_{H,j}^{\mu^{\text{trial}}} \rangle}{1 - D_j^{\mu^{\text{trial}}}} - \langle -\sigma_{H,j}^{\mu^{\text{trial}}} \rangle\right]\mathbb{I}. \tag{22}$$

The elastic predictor step, thus obtained, must be verified by calculating the yield function $f_j^{\mu^{\text{trial}}}$. If $f_j^{\mu^{\text{trial}}} \leq 0$, there is no growth of micro-plasticity nor micro-damage, therefore the predictor stage need not be corrected. Otherwise, if $f_j^{\mu^{\text{trial}}} > 0$, plastic corrector step must be employed. In the corrector step the following set of equations is solved

$$f_j^{\mu} = 0, \tag{23a}$$

$$\boldsymbol{\varepsilon}_j^{\mu,e} = \boldsymbol{\varepsilon}_j^{\mu,e^{\text{trial}}} + (\gamma - 1)(\boldsymbol{\varepsilon}_j^{\mu,p} - \boldsymbol{\varepsilon}_j^{\mu,p^{\text{trial}}}), \tag{23b}$$

$$\boldsymbol{\varepsilon}_j^{\mu,p} = \boldsymbol{\varepsilon}_j^{\mu,p^{\text{trial}}} + \frac{3}{2}\frac{\tilde{\boldsymbol{\sigma}}^{\mu} - \boldsymbol{\beta}^{\mu}}{(\tilde{\boldsymbol{\sigma}}^{\mu} - \boldsymbol{\beta}^{\mu})_{eq}}\frac{\Delta\lambda_j}{1 - D_j^{\mu}}, \tag{23c}$$

$$p_j^{\mu} = p_j^{\mu^{\text{trial}}} + \frac{\Delta\lambda_j}{1 - D_j^{\mu}}, \tag{23d}$$

$$\boldsymbol{\alpha}_j^{\mu} = \boldsymbol{\alpha}_j^{\mu^{\text{trial}}} + \frac{3}{2}\frac{\tilde{\boldsymbol{\sigma}}^{\mu} - \boldsymbol{\beta}^{\mu}}{(\tilde{\boldsymbol{\sigma}}^{\mu} - \boldsymbol{\beta}^{\mu})_{eq}}\Delta\lambda_j, \tag{23e}$$

$$D_j^{\mu} = D_j^{\mu^{\text{trial}}} + \left(\frac{Y_j^{\mu}}{S}\right)^{s}\frac{\Delta\lambda_j}{1 - D_j^{\mu}}, \tag{23f}$$

$$Y_j^{\mu} = R_v\frac{(\tilde{\sigma}_{eq_j}^{\mu})^2}{2E}, \tag{23g}$$

$$\boldsymbol{\beta}_j^{\mu} = Q\boldsymbol{\alpha}_j^{\mu}. \tag{23h}$$

Non-linear solvers, such as the Newton-Raphson method can be used to solve such coupled non-linear set of equations. Once converged, the damage at the macro-scale can be updated as

$$\hat{D}_j = 1 - (1 - D_j^{\mu})^{\varphi}. \tag{24}$$

Once the nodal cycle of interest has been investigated, the macro-quantities $\hat{\sigma}$ and $\hat{\varepsilon}$ are fed to the global stage where the admissibility conditions are solved.

2.5.2. Latin global stage using model order reduction

The transfer of information from the local stage to the global stage is through the search direction equation

$$(\boldsymbol{\varepsilon}_{i+1} - \hat{\boldsymbol{\varepsilon}}_{i+1/2}) = \mathbf{H}^{-}(\boldsymbol{\sigma}_{i+1} - \hat{\boldsymbol{\sigma}}_{i+1/2}), \tag{25}$$

with the search direction operator $\mathbf{H}^{-} = \mathbf{C}^{-1}$ as the structure is macroscopically elastic.

The boundary conditions being already taken into account in the initialisation, the objective herein is to update the quantities of interest in terms of corrections, which read

$$\Delta\boldsymbol{\sigma}_{i+1} = \boldsymbol{\sigma}_{i+1} - \boldsymbol{\sigma}_i, \quad \Delta\boldsymbol{\varepsilon}_{i+1} = \boldsymbol{\varepsilon}_{i+1} - \boldsymbol{\varepsilon}_i, \quad \Delta u_{i+1} = u_{i+1} - u_i. \tag{26}$$

The static admissibility condition, eq. (1), for a given nodal cycle when written in terms of corrections, reads

$$\int_{\Omega\times[\Theta_m,\Theta_m+\Delta T]} \Delta\boldsymbol{\sigma}_{i+1} : \boldsymbol{\varepsilon}^{*} d\Omega\, dt = 0, \tag{27}$$

for any $\boldsymbol{\varepsilon}^{*}$ kinematically admissible to zero. The search direction equation defined by eq. (25) may be re-written in terms of corrections as

$$\Delta\boldsymbol{\sigma}_{i+1} = \mathbf{C}\Delta\boldsymbol{\varepsilon}_{i+1} + (\hat{\boldsymbol{\sigma}}_{i+1/2} - \boldsymbol{\sigma}_i) - \mathbf{C}(\hat{\boldsymbol{\varepsilon}}_{i+1/2} - \boldsymbol{\varepsilon}_i). \tag{28}$$

Equation (27) along with eq. (28) produce the following weak form

$$\int_{\Omega\times[\Theta_m,\Theta_m+\Delta T]} \mathbf{C}\Delta\boldsymbol{\varepsilon}_{i+1} : \boldsymbol{\varepsilon}^{*} d\Omega\, dt = \int_{\Omega\times[\Theta_m,\Theta_m+\Delta T]} \mathbf{C}(\hat{\boldsymbol{\varepsilon}}_{i+1/2} - \boldsymbol{\varepsilon}_i) : \boldsymbol{\varepsilon}^{*} d\Omega\, dt - \int_{\Omega\times[\Theta_m,\Theta_m+\Delta T]} (\hat{\boldsymbol{\sigma}}_{i+1/2} - \boldsymbol{\sigma}_i) : \boldsymbol{\varepsilon}^{*} d\Omega\, dt. \tag{29}$$

The high numerical cost for solving this weak form can be reduced by using PGD-based model reduction approaches, as commonly used in the global stage of LATIN (see Ladevèze, 1999; Chinesta and Ladevèze, 2014).

PGD is based on the idea of separation of variables over generalised coordinates, e.g. space and time. The approximations of the quantities

Table 1
Material properties for Cr–Mo steel at 20°C as given in Lemaitre and Desmorat (2005).

E	200000 MPa
ν	0.3
C	6000 MPa
s	2
S	2.8 MPa
σ_f^{∞}	140 MPa
σ_y	180 MPa

of interest can thereby be written as the sum of products of functions of space and time. The separated representation, when introduced in the governing equation, decomposes it into sovereign spatial and temporal problems, which can then be solved independently using fixed point method.

For the current problem of interest, at a given LATIN iteration $i+1$ the nodal degrees of freedom can be approximated as

$$\boldsymbol{u}_{i+1} = \boldsymbol{u}_0 + \sum_{j=1}^{n} \lambda_j(t)\bar{\boldsymbol{u}}_j(\underline{x}), \tag{30}$$

with the corresponding strain field written as

$$\boldsymbol{\varepsilon}_{i+1} = \boldsymbol{\varepsilon}_0 + \sum_{j=1}^{n} \lambda_j(t)\bar{\boldsymbol{\varepsilon}}_j(\underline{x}), \tag{31}$$

where the terms $\boldsymbol{u}_0$ and $\boldsymbol{\varepsilon}_0$ represent the initial solution for the displacement and total strain, respectively, $\{\lambda_j\}_{j=1}^n$ is a set of time functions, and $\{\bar{\boldsymbol{u}}_j\}_{j=1}^n$ and $\{\bar{\boldsymbol{\varepsilon}}_j\}_{j=1}^n$ are set of space functions such that

$$\bar{\boldsymbol{\varepsilon}}_j(\underline{x}) = \mathbf{B}^T\bar{\boldsymbol{u}}_j(\underline{x}),\ j \in [1, n], \tag{32}$$

where $\mathbf{B}$ is a matrix containing the derivatives of the shape functions.

For a given LATIN iteration, the corrective terms are calculated using a maximum of one PGD-pair. If at LATIN iteration i, n PGD pairs have been generated and the objective in iteration $i+1$ is to generate one more couple, the corrective terms can be written as

$$\begin{aligned}\Delta\boldsymbol{u}_{i+1}(\underline{x}, t) &= \lambda_{n+1}(t)\bar{\boldsymbol{u}}_{n+1}(\underline{x}),\\ \Delta\boldsymbol{\varepsilon}_{i+1}(\underline{x}, t) &= \lambda_{n+1}(t)\bar{\boldsymbol{\varepsilon}}_{+1}(\underline{x}).\end{aligned} \tag{33}$$

Incorporation of these separated forms in eq. (29), with $\boldsymbol{\varepsilon}^* = \lambda^*\bar{\boldsymbol{\varepsilon}}(\underline{x}) + \lambda(t)\bar{\boldsymbol{\varepsilon}}^*$, leads to separated spatial and temporal problems. The spatial problem is given by

$$\int_{\Omega} \langle\lambda_{m+1}\lambda_{m+1}\rangle\mathbf{C}\bar{\boldsymbol{\varepsilon}}\colon\bar{\boldsymbol{\varepsilon}}^* d\,\Omega = \int_{\Omega} \langle\lambda_{m+1}\rangle\bar{\Delta}^{\varepsilon}\colon\bar{\boldsymbol{\varepsilon}}^* d\Omega \tag{34}$$

with $\langle\cdot\rangle = \int_{[\Theta_m,\Theta_{m+\Delta T}]} \cdot\, dt$, $\bar{\Delta}^{\varepsilon} = \mathbf{C}(\hat{\boldsymbol{\varepsilon}}_{i+1/2} - \boldsymbol{\varepsilon}_i) - (\hat{\boldsymbol{\sigma}}_{i+1/2} - \boldsymbol{\sigma}_i)$ and for all $\bar{\boldsymbol{\varepsilon}}^*$ kinematically admissible to zero. This is a classical boundary value problem that can be solved using finite element discretisation.

The temporal problem is obtained as

$$\int_{[\Theta_m,\Theta_{m+\Delta T}]} \left(\int_{\Omega} \mathbf{C}\bar{\boldsymbol{\varepsilon}}_{n+1}\colon\bar{\boldsymbol{\varepsilon}}_{n+1} d\Omega\right)\lambda_{n+1}\lambda^* dt = \int_{[\Theta_m,\Theta_{m+\Delta T}]} \left(\int_{\Omega} \Delta^{\varepsilon}\colon\bar{\boldsymbol{\varepsilon}}_{n+1} d\Omega\right)\lambda^* dt, \tag{35}$$

with no conditions on λ^*. This boils down to an algebraic equation given by

$$\left(\int_{\Omega} \mathbf{C}\bar{\boldsymbol{\varepsilon}}_{n+1}\colon\bar{\boldsymbol{\varepsilon}}_{n+1} d\Omega\right)\lambda_{n+1} = \int_{\Omega} \Delta^{\varepsilon}\colon\bar{\boldsymbol{\varepsilon}}_{n+1} d\Omega. \tag{36}$$

This spatio-temporal problem can be expensive as the calculation of the spatial part is costly, hence it is advised to add a new space-time pair only if necessary. In most cases, the same spatial basis vectors can be reused and the time functions can just be updated to obtain the corrective quantities of interest. For a given LATIN iteration $i+1$, the quantities of interest can be approximated as

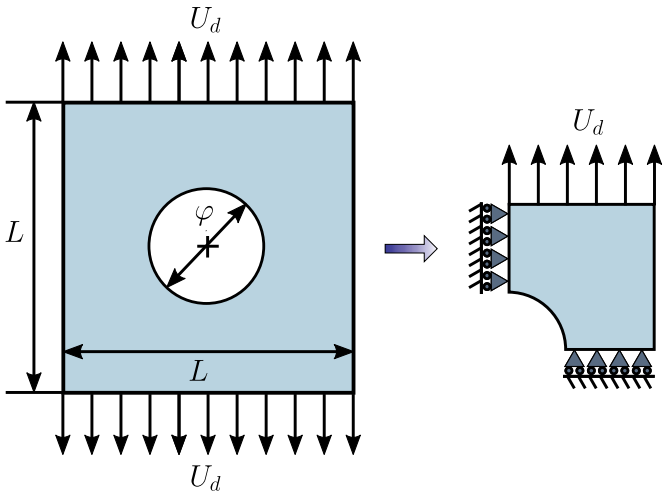

Fig. 6. A rectangular plate with circular hole, subjected to specified distributed displacements.

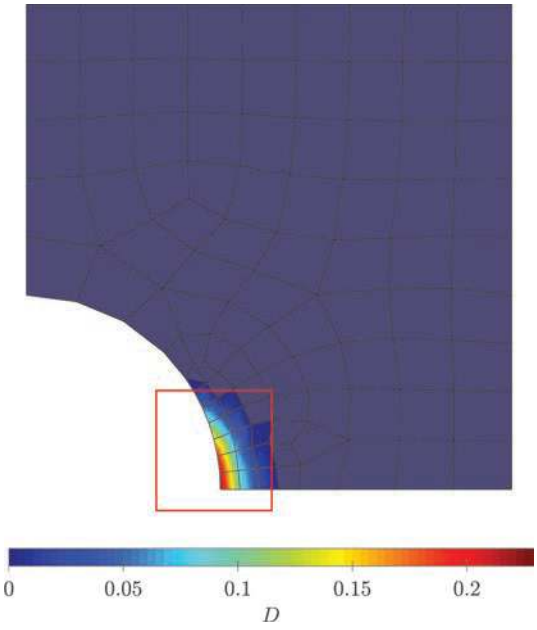

Fig. 7. Distribution of damage at the macro-scale after macroscopic critical value is reached.

$$\begin{aligned}\Delta\boldsymbol{u}_{i+1}(\underline{x}, t) &= \textstyle\sum_{j=1}^{n} \Delta\lambda_j(t)\bar{\boldsymbol{u}}_j(\underline{x}),\\ \Delta\boldsymbol{\varepsilon}_{i+1}(\underline{x}, t) &= \textstyle\sum_{j=1}^{n} \Delta\lambda_j(t)\bar{\boldsymbol{\varepsilon}}_j(\underline{x}),\end{aligned} \tag{37}$$

where $\{\Delta\lambda_j\}_{j=1}^m$ are the corrections to the time functions, and the space functions are known from previous iterations. Such approximations when introduced in eq. (29), lead to a temporal problem written as

$$\boldsymbol{\Lambda} = \mathbf{G}^{-1}\mathbf{P} \tag{38}$$

with

$$\boldsymbol{\Lambda}_{ij} = \Delta\lambda_i(t_j), \tag{39a}$$

$$\mathbf{G}_{ij} = \int_{\Omega} \bar{\boldsymbol{\varepsilon}}_i(\underline{x})\colon\mathbf{C}\bar{\boldsymbol{\varepsilon}}_j(\underline{x})\, d\Omega, \tag{39b}$$

$$\mathbf{P}_{ij} = \int_{\Omega} \Delta^{\varepsilon}(x, t_j)\colon\bar{\boldsymbol{\varepsilon}}_i(\underline{x})\, d\Omega. \tag{39c}$$

This update step is very cheap and needs only to solve a linear system of equations.

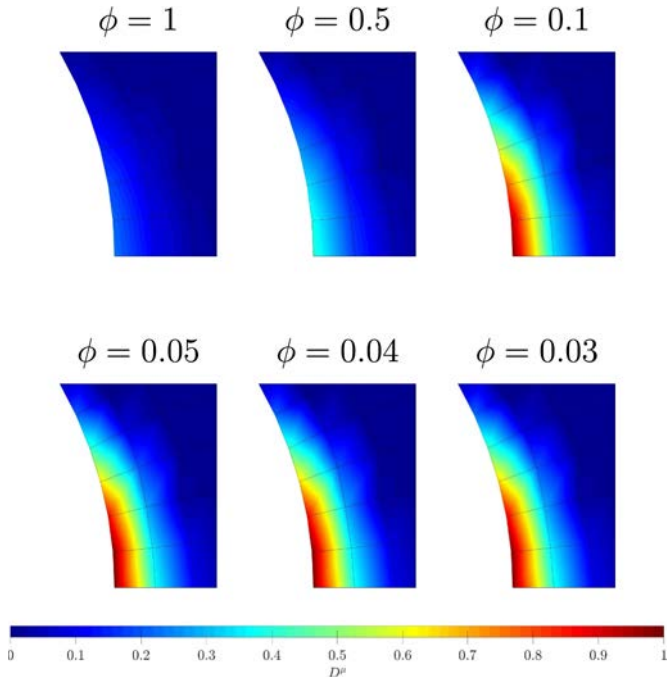

Fig. 8. Distribution of damage at the micro-scale after macroscopic critical value is reached for different values of φ

The global stage of the LATIN method generally starts with this update step where the temporal basis is updated by reusing the spatial basis built by the greedy algorithm during previous iterations. The reduced order model, hence obtained, if not satisfactory, is improved through the enrichment step where a new space-time pair is calculated. There have been several criteria to decide whether enrichment stage is required or not (see Relun et al., 2011; Bhattacharyya et al., 2018a; Bhattacharyya, 2018). In the current context, if the maximum norm of the temporal corrections $\{\Delta\lambda_j\}_{j=1}^m$ is less than a pre-defined tolerance, a new couple is added. Once the strain correction is obtained, the stress correction can be calculated using eq. (28).

The convergence of the LATIN method can be measured using a dedicated error indicator which is given by

$$\xi = \frac{||\hat{\boldsymbol{s}}^p_{i+1/2} - \boldsymbol{s}^p_{i+1}||}{\hat{\boldsymbol{s}}^p_{i+1/2} + \boldsymbol{s}^p_{i+1}}, \tag{40}$$

with

$$||\boldsymbol{s}^p||^2 = \int_{[0,T]\times\Omega} (\boldsymbol{\sigma}: \mathbf{C}^{-1}\boldsymbol{\sigma} + \boldsymbol{\varepsilon}: \mathbf{C}\boldsymbol{\varepsilon})\, d\Omega\, dt. \tag{41}$$

If this indicator is below a certain tolerance, the given nodal cycle has reached convergence and the algorithm moves to the next nodal cycle.

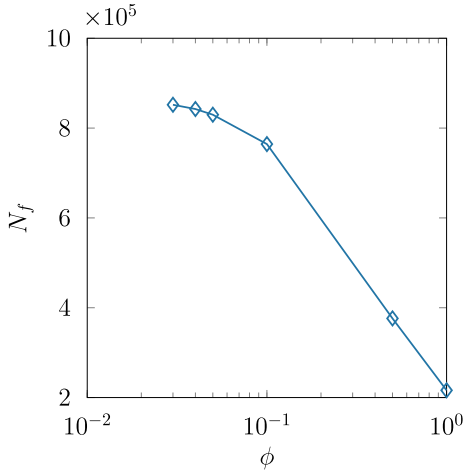

Fig. 10. Influence of the parameter φ on the number of cycles before reaching crack initiation (N_f).

2.6. Temporal interpolation

To calculate nodal cycle $m+1$ after the computation of nodal cycle m, there are two problems that need addressing. The first is to evaluate the length of the temporal element, i.e. the value of Θ_{m+1}. It is possible, of course to use uniform temporal mesh size as done in Bhattacharyya et al. (2018b), however an adaptive scheme is pertinent to obtain an optimum balance between expense and accuracy. Therefore an adaptive scheme similar to the classical jump cycle algorithm (see Lemaitre and Doghri, 1994b) is proposed as

$$\tilde{N} = 2 + \min\left(\frac{\overline{\Delta D}}{\frac{\delta D}{\delta N}|_m}\right), \tag{42}$$

where $\overline{\Delta D} = \frac{D_c}{50}$ and $\frac{\delta D}{\delta N}|_m$ represents the growth of macro-damage in the nodal cycle m and $\tilde{N}$ is the total number of cycles within the time element including both nodal cycles m and $m+1$. Hence, $(\tilde{N}-2)$ is the number of cycles to be jumped over.

The second issue is to determine the initial conditions, i.e. the quantities of interest at Θ_{m+1}, required at the local stage. The final values at nodal cycle m, i.e. values at $\Theta_m + \Delta T$, for the cyclic quantities of interest such as $\hat{\varepsilon}$, $\varepsilon^{\mu,e}$, $\varepsilon^{\mu,p}$, $\boldsymbol{\alpha}^\mu$, $\boldsymbol{\beta}^\mu$, $\boldsymbol{\sigma}^\mu$ are considered to be the initial values at nodal cycle $m+1$. For the quantities of interest which are not cyclic such as cumulative plastic strain p^μ and damage D and D^μ, the initialisation can be obtained through linear extrapolation. These extrapolations can be represented as

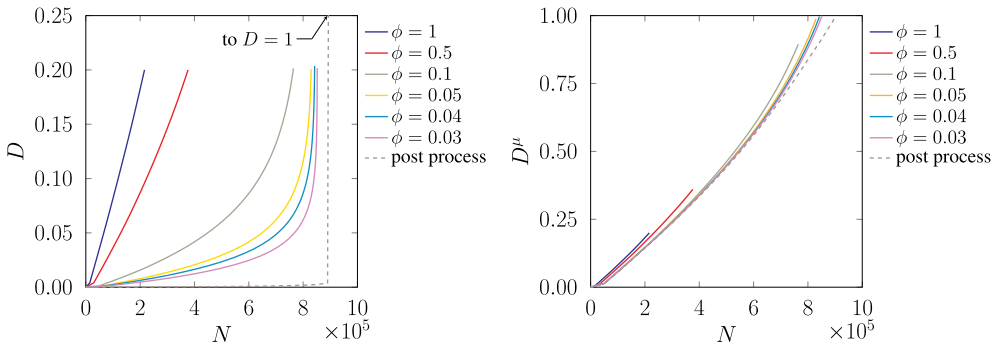

(a) Macro-damage evolution (b) Micro-damage evolution

Fig. 9. Damage evolutions for different values of φ

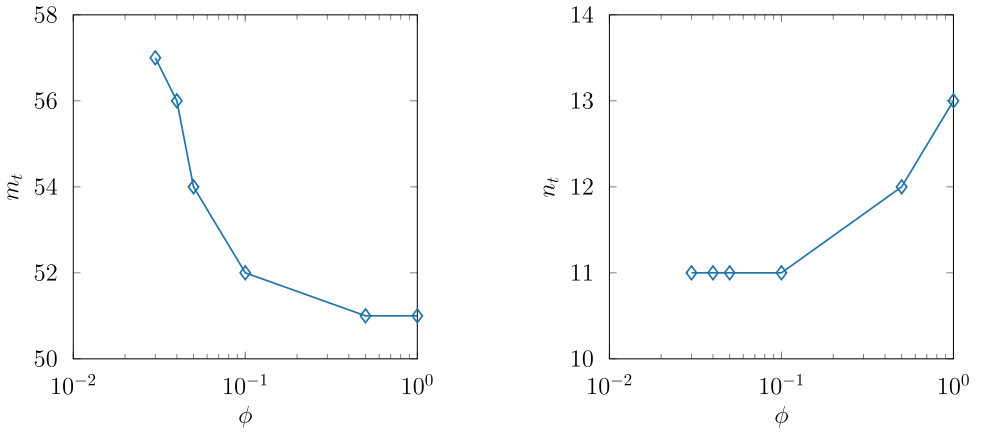

(a) Number of nodal cycles m_t (b) Number of generated PGD-modes n_t

Fig. 11. Numerical behaviour of the multi-scale LATIN-PGD algorithm for different values of φ

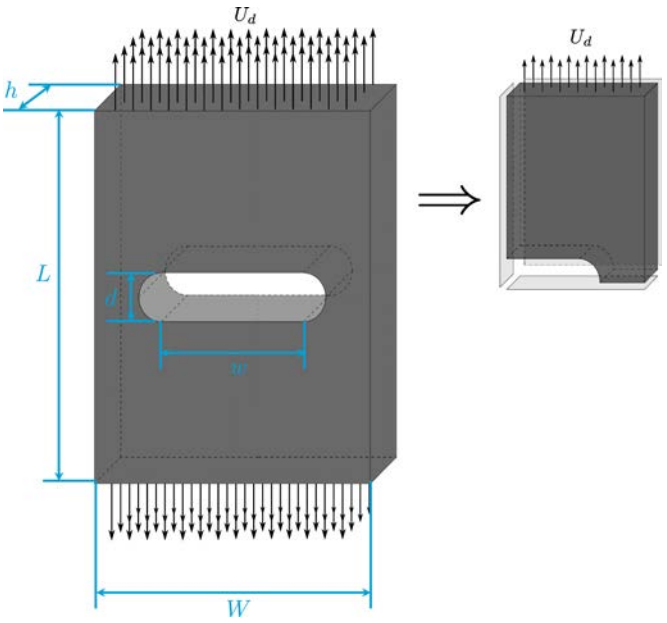

Fig. 12. A block with a central groove subjected to distributed loading.

$$D(\Theta_{m+1}) = D(\Theta_m + \Delta T) + (\tilde{N} - 2)\Delta D_m, \tag{43a}$$

$$D^{\mu}(\Theta_{m+1}) = D^{\mu}(\Theta_m + \Delta T) + (\tilde{N} - 2)\Delta D^{\mu}_m, \tag{43b}$$

$$p^{\mu}(\Theta_{m+1}) = p^{\mu}(\Theta_m + \Delta T) + (\tilde{N} - 2)\Delta p^{\mu}_m, \tag{43c}$$

with Δp^{μ}_m, ΔD^{μ}_m, and ΔD_m being the increments at the nodal cycle m. This idea of linear extrapolation might be inaccurate, especially if $\tilde{N}$ is large. Therefore, the initial guess of the initial conditions are obtained from eq. (43), and thereafter the initial conditions are improved using the idea proposed in Bhattacharyya et al. (2018c). This boils down to an update of the initial conditions at each LATIN iteration where these conditions are recomputed based on

$$D(\Theta_{m+1}) = D(\Theta_m) + \Delta D_m + \sum_{k=1}^{\tilde{N}-2} \Delta D_k, \tag{44a}$$

$$D^{\mu}(\Theta_{m+1}) = D^{\mu}(\Theta_m) + \Delta D^{\mu}_m + \sum_{k=1}^{\tilde{N}-2} \Delta D^{\mu}_k, \tag{44b}$$

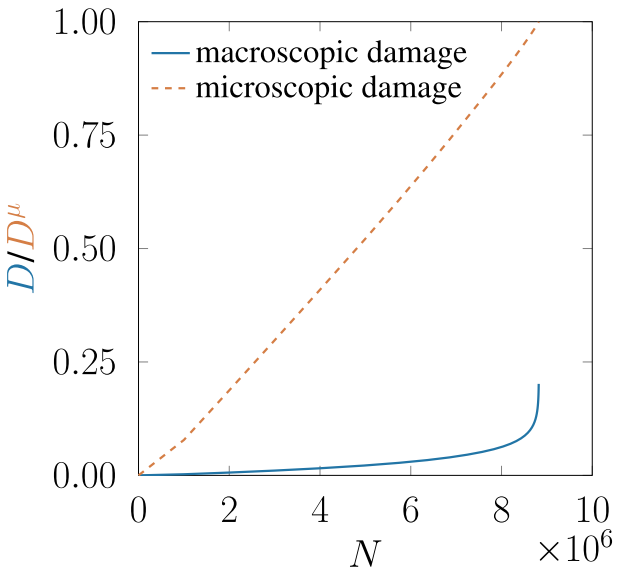

Fig. 13. Evolution of damage at the weakest Gauss point for both length scales ($\varphi = 0.03$).

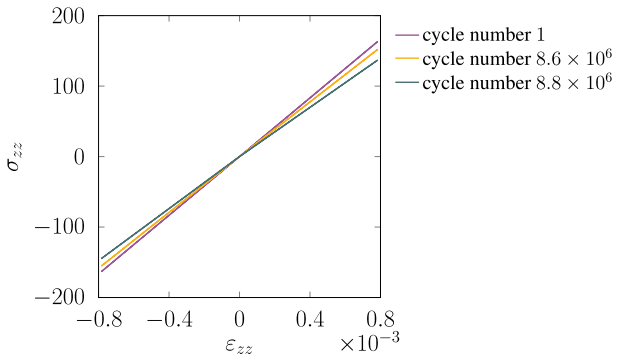

Fig. 14. Stress-strain diagram at certain cycles at the macro-scale.

$$p^{\mu}(\Theta_{m+1}) = p^{\mu}(\Theta_m) + \Delta p^{\mu}_m + \sum_{k=1}^{\tilde{N}-2} \Delta p^{\mu}_k, \tag{44c}$$

where $\Delta\bullet_m$ represents the increments at nodal cycle m and $\Delta\bullet_k$ is the increment at each intermediate cycle. To bypass the computation time needed to acquire all the increments, the increments at nodal cycle m

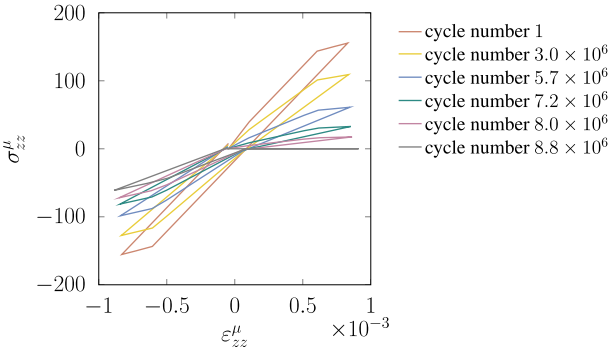

Fig. 15. Stress-strain diagram at certain cycles at the micro-scale.

and $m+1$, i.e. ΔD_m and ΔD_{m+1}, are used to approximate $\Delta\bullet_k$ using an interpolation scheme. In such a scheme, linear shape functions in the slow time scale can be defined as

$$\nu_m(\theta_k) = \frac{\Theta_{m+1} - \theta_k}{\Theta_{m+1} - \Theta_m}, \quad \nu_{m+1}(\theta_k) = \frac{\theta_k - \Theta_m}{\Theta_{m+1} - \Theta_m}, \quad \forall\, t \in [\Theta_m, \Theta_{m+1} + \Delta T]. \tag{45}$$

Using this assumption, the initial conditions for the "nodal cycle" $m+1$ can be written as

$$D(\Theta_{m+1}) = D(\Theta_m) + \sum_{k=0}^{\tilde{N}-2} (\nu_m(\theta_k)\Delta D_m + \nu_{m+1}(\theta_k)\Delta D_{m+1}), \tag{46a}$$

$$D^\mu(\Theta_{m+1}) = D^\mu(\Theta_m) + \sum_{k=0}^{\tilde{N}-2} (\nu_m(\theta_k)\Delta D^\mu_m + \nu_{m+1}(\theta_k)\Delta D^\mu_{m+1}), \tag{46b}$$

$$p^\mu(\Theta_{m+1}) = p^\mu(\Theta_m) + \sum_{k=0}^{\tilde{N}-2} (\nu_m(\theta_k)\Delta p^\mu_m + \nu_{m+1}(\theta_k)\Delta p^\mu_{m+1}). \tag{46c}$$

Once the nodal cycles m and $m+1$ have been calculated, shape functions as previously defined in eq. (45) are used to interpolate the solution set

$$\boldsymbol{s}(t = \theta_k + \tau_k) = \nu_m(\theta_k)\boldsymbol{s}(\Theta_m + \tau_m) + \nu_{m+1}(\theta_k)\boldsymbol{s}(\Theta_{m+1} + \tau_{m+1}), \forall\, t \in [\Theta_m, \Theta_{m+1} + \Delta T]. \tag{47}$$

The process is pursued subsequently for every temporal element over the whole time domain or till the critical damage is reached.

3. Numerical examples

The proposed two-scale damage model in the multi-temporal LATIN-PGD framework is tested on several academic examples. The goal of the analyses is to estimate the number of surviving cycles before reaching the critical damage value $D_c = 0.2$ at the macroscopic scale. The material considered is a Cr–Mo steel at 20°C, the properties of which are given in Table 1. The loading for each analysis is such that the equivalent stress is between the macroscopic yield stress and the asymptotic fatigue limit such there is no macro-plasticity and plasticity exits only at micro-scale.

3.1. Plate with a hole

The first set of analyses is on a two-dimensional square plate with a circular hole subjected to distributed sinusoidal displacements as represented in Fig. 6. The geometry of the structure is defined by the length of each side $L = 100$ mm and the diameter of the circular hole $\phi = 40$ mm. The prescribed displacement is of the form $U_d = U_0 \sin\left(\frac{2\pi t}{\Delta T}\right)$ with the amplitude $U_0 = 0.025$ mm and the time period $\Delta T = 10$ s. The spatial discretisation is done using 96 linear isoparametric quadrilateral elements with four Gauss points per element. The time-step size used for the fine time discretisation is 1 s.

This set of analyses aims at investigating the number of survival cycles N_f for different values of the coupling parameter φ. Six different tests are conducted with values of φ being 1, 0.5, 0.1, 0.05, 0.04, 0.03, respectively, and the LATIN-PGD algorithm continues till the macroscopic damage reaches the critical value 0.2.

The macroscopic damage distributions after D_c value is reached are found to be the same for all the values of φ, one of which is shown in Fig. 7 along with the region of interest.

The micro-damage contour at the region of interest is shown in Fig. 8 for different values of φ. The higher the coupling, the lower the value of the microscopic damage when the macroscopic damage reaches 0.2.

The evolution of damage with respect to number of cycles for the weakest Gauss point for different values of φ at both length scales is shown in Fig. 9. Lower the values of φ, higher is the number of survival cycles. For lower values of φ, the macroscopic damage value remains low for most of the life time and later on there is a drastic increase in

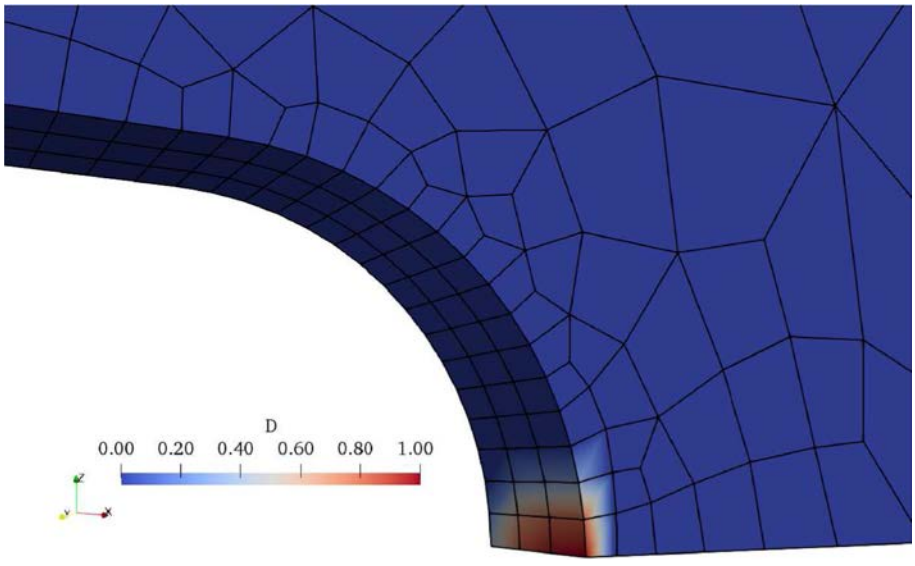

Fig. 16. Distribution of damage at the micro-scale at $D_{max} = D_c$.

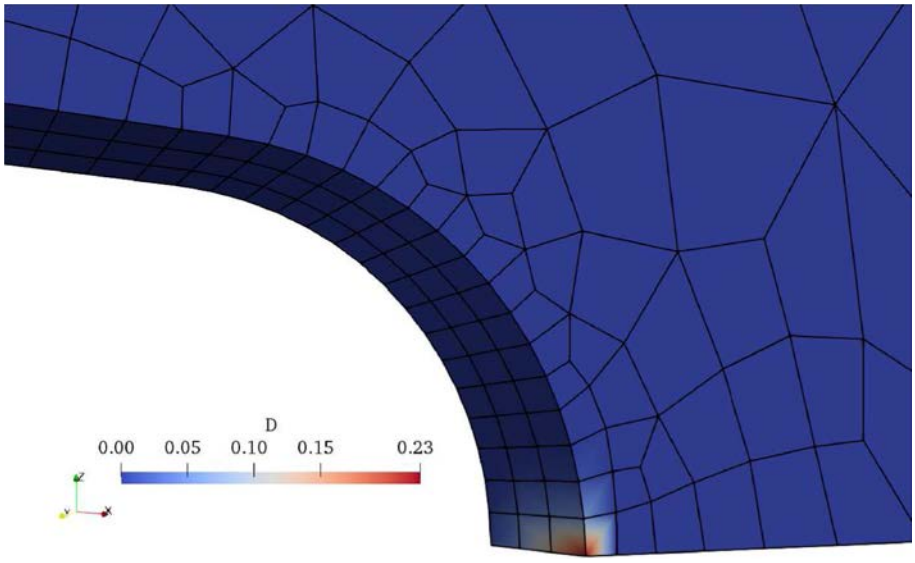

Fig. 17. Distribution of damage at the macro-scale at $D_{max} = D_c$.

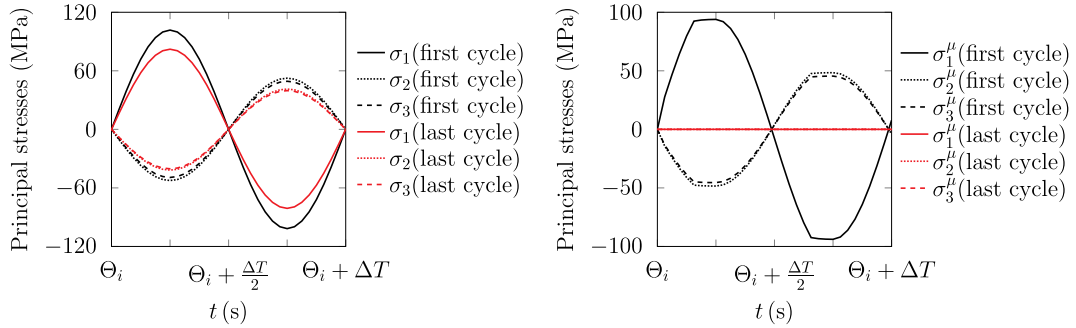

(a) Macro-principal stresses (b) Micro-principal stresses

Fig. 18. Evolution of principal stresses with respect to time during the first cycle ($\Theta_i + \Delta T = 10$ s), and the last cycle ($\Theta_i + \Delta T = 8.8 \times 10^7$ s), at the weakest Gauss point.

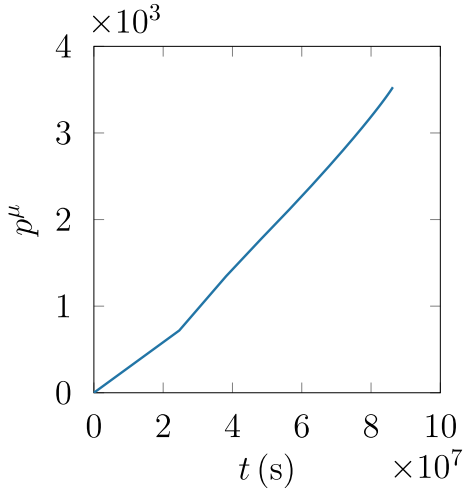

Fig. 19. Evolution of the cumulative plastic strain p^μ with respect to time at the weakest Gauss point.

damage. As far as the micro-damage evolutions are concerned, for lower values of φ, the final values reach close to 1 when the macroscopic values reach D_c. For the sake of comparison, a post-processed solution is calculated, considering a very low value of φ. In such cases the macroscopic damage shows no visible evolution for the entire lifetime and suddenly reaches the value of one when the microscopic damage reaches one. For exact post-processing (see Lemaitre and Desmorat, 2005, for instance), $\varphi = 0$, and $D = 1$, when $D^\mu = 1$, and zero otherwise. The idea therein is microscopic damage will have no influence on the macroscopic behaviour and failure will occur all of a sudden. In this case the value of φ considered as post-processed results is 10^{-3} and not exact zero, to avoid numerical discrepancies. However, the aforementioned idea can still be reflected (see Fig. 9), and with decrease in the coupling parameter the damage curves will asymptotically reach the post-processed curves.

The increase in the total number of survival cycles with decrease in the values of φ is represented in Fig. 10. Fig. 11a shows the fact that the number of nodal cycles required for the simulation decreases with increase in φ. The total number of PGD modes required increases with increase in φ as shown in Fig. 11b. For lower values of φ the coupling between macro- and micro-damage is reduced, hence higher micro-damage value is required to achieve macroscopic critical damage value. To achieve this higher microscopic damage, the number of cycles required is higher. Also for lower values of φ the gradients are much higher towards the end of the structural life time (see Fig. 9a), thereby the number of nodal cycles is higher. For higher values of φ, the non-linearities introduced in the macro-scale are higher, leading to higher number of PGD modes.

To summarise the two-dimensional analysis, the value of $\varphi = 0.03$ mimics the intended macro-micro behaviour most effectively, i.e. D^μ approaches the closest to 1, when D reaches 0.2. This value of φ is used in the next three-dimensional numerical example.

3.2. Block with a groove

This analysis is on a cuboidal structure with a central groove as shown in Fig. 12. The geometry of the structure is defined by the dimensions of the cuboid, i.e. $L = 40$ mm, $W = 20$ mm and $h = 2$ mm, and the dimensions of the groove, i.e. $d = 4$ mm and $w = 6$ mm. The structure is subjected to uniformly distributed displacements of the form $U_d = U_0 \sin\left(\frac{2\pi t}{\Delta T}\right)$ with the amplitude $U_0 = 0.004$ mm and the time period $\Delta T = 10$ s. Considering symmetric boundary conditions, only $1/8$ of the block is used for analysis.

The structure is discretised in space using 387 linear eight-noded isoparametric brick elements with eight Gauss points per element. Such spatial discretisation produces a total of 628 nodes and 3096 Gauss points. For the temporal part, the time step size used for the fine time discretisation is $10/32$ s. Cyclic loading is applied to the structure till the macroscopic damage reaches the critical value 0.2 for $\varphi = 0.03$.

The analysis resulted in a total number of surviving cycles $N_f = 8.8 \times 10^6$ for a macroscopic damage value of 0.2, with 38 nodal cycles and 9 PGD modes. The usage of $\varphi = 0.03$ resulted in the microscopic damage value to be close to 1 when the macroscopic value reaches 0.2. The evolution of damage for both length scales at the weakest Gauss point is shown in Fig. 13.

The obvious decrease in the slope of the stress-strain diagram with damage evolution for the macro-scale at the weakest Gauss point can be seen in Fig. 14. Here, the curves plotted for certain cycles, belong to the normal stress and normal strain of the z-component, i.e. σ_{zz} and ε_{zz}. Evidently, the continuous stress-strain response shows an elastic behaviour, with decrease in slope, representing the damage behaviour. The behaviour due to unilateral condition although exists, is relatively less profound at the macro-scale.

The microscopic stress-strain behaviour, i.e. σ^{μ}_{zz}-ε^{μ}_{zz}, represented in Fig. 15 shows the hysteretic behaviour due to micro-plasticity. The decrease of the slope of the stress-strain diagrams is profound with increase in number of load cycles. The unilateral behaviour is also captured nicely, with profound difference in slope for the tensile and compressive parts. Even for the case where the microscopic damage reaches 1, the load carrying capacity in the compressive part still exists, whereas the load carrying capacity for the tensile part vanishes.

The damage distributions at the end of loading for both length scales are depicted in Figs. 16 and 17, showing localisation of the quantity of interest.

The principal stresses, for the Gauss point with maximum damage, as plotted in Fig. 18, show two interesting features. First of all, the macroscopic principal stresses (Fig. 18a) are smooth sinusoidal in nature, depicting the elastic macroscopic behaviour, however their microscopic counterparts are not (Fig. 18b), exhibiting the presence of plasticity at the micro-scale. Secondly, the amplitudes are drastically reduced for the microscopic principal stresses from the first to the last cycle (Fig. 18b), as compared to their macroscopic counterparts (Fig. 18a). This is in coherence with the behaviour shown in Figs. 14 and 15, i.e. the drastic reduction in load carrying capacity of the micro-scale compared to the macro-scale. It must be emphasised that although the responses presented in this article are proportional in nature, the damage model due to its kinetic nature, and the numerical strategy, are not restrictive and so also applicable for non-proportional loadings and responses. Finally the cumulative plastic strain for the weakest Gauss point is plotted in Fig. 19 with respect to time and its evolution follows a similar behaviour as that of the microscopic damage.

4. Conclusion

In this paper, high-cycle fatigue computations based on two-scale damage model have been developed in the LATIN-PGD framework. A two-scale damage model has been considered with a feedback of the micro-scale damage growth on the macro-scale elastic behaviour. Both fully coupled and uncoupled -by post-processing- two-scale damage modelling have been presented. A continuous transition coupled/uncoupled is obtained thanks to the volume fraction parameter φ. A two-temporal scale scheme based on finite element like description in time has been used to reduce the actual number of cycles which are calculated by satisfying the global admissibilities and the local constitutive behaviour through the LATIN-PGD technique. The numerical framework has proven efficient for different academic examples. This efficient numerical framework opens the door to numerical simulations for complex loading cases, i.e. random fatigue, and large three-dimensional structures thanks to both the kinetic (rate) nature of the damage modelling and the model order reduction capacities.

Acknowledgements

The support by the German Research Foundation (DFG) via IRTG 1627 is highly appreciated.

References

Allix, O., Ladevèze, P., Gilleta, D., Ohayon, R., 1989. A damage prediction method for composite structures. Int. J. Numer. Methods Eng. 27 (2), 271–283.
Berveiller, M., Zaoui, A., 1979. An extension of the self-consistent scheme to plastically flowing polycrystal. J. Mech. Phys. Solids 26, 325–344.
Besson, J., Cailletaud, G., Chaboche, J.-L., Forest, S., Blétry, M., 2010. Non-linear Mechanics of Materials. Springer.
Bhamare, S., Eason, T., Spottswood, S., Mannava, S.R., Vasudevan, V.K., Qian, D., 2014. A multi-temporal scale approach to high cycle fatigue simulation. Comput. Mech. 53 (2), 387–400.
Bhattacharyya, M., 2018. A Model Reduction Approach in Space and Time for Fatigue Damage simulation. Ph.D. thesis. École Normale Supérieure Paris-Saclay, Leibniz Universität Hannover.
Bhattacharyya, M., Fau, A., Nackenhorst, U., Néron, D., Ladevèze, P., 2018a. A Latin-based model reduction approach for the simulation of cycling damage. Comput. Mech. 62 (4), 725–743.
Bhattacharyya, M., Fau, A., Nackenhorst, U., Néron, D., Ladevèze, P., 2018b. A model reduction technique in space and time for fatigue simulation. In: Sorić, J., Wriggers, P., Allix, O. (Eds.), Multiscale Modeling of Heterogeneous Structures. Springer International Publishing, Cham, pp. 183–203.
Bhattacharyya, M., Fau, A., Nackenhorst, U., Néron, D., Ladevèze, P., 2018c. A multi-temporal scale model reduction approach for the computation of fatigue damage. Comput. Methods Appl. Mech. Eng. 340, 630–656.
Burlon, S., Mroueh, H., Cao, J., 2014. 'skipped cycles' method for studying cyclic loading and soil–structure interface. Comput. Geotech. 61, 209–220.
Chaboche, J.L., Lesne, P.M., 1988. A non-linear continuous fatigue damage model. Fatigue Fract. Eng. Mater. Struct. 11 (1), 1–17.
Chinesta, F., Ladevèze, P. (Eds.), 2014. Separated Representations and PGD-Based Model Reduction: Fundamentals and Applications. Springer Vienna, pp. 91–152 Ch. PGD in linear and nonlinear Computational Solid Mechanics.
Cognard, J.-Y., Ladevèze, P., 1993. A large time increment approach for cyclic visco-plasticity. Int. J. Plast. 9 (2), 141–157.
Dang Van, K., 1999. Introduction to fatigue analysis in mechanical design by the multi-scale Approach. In: International Centre for Mechanical Sciences (Courses and Lectures). vol. 392. Springer, Vienna, pp. 57–88.
Dascalu, C., 2009. A two-scale damage model with material length. C.R. Mecanique 337, 645–652.
Desmorat, R., 2002. Fast estimation of localized plasticity and damage by energetic methods. Int. J. Solids Struct. 39 (12), 3289–3310.
Desmorat, R., Cantournet, S., 2008. Modeling microdefects closure effect with isotropic/anisotropic damage. Int. J. Damage Mech. 17 (1), 65–96.
Desmorat, R., Kane, A., Seyedi, M., Sermage, J., 2007. Two scale damage model and related numerical issues for thermo-mechanical High Cycle Fatigue. Eur. J. Mech. A Solid. 26 (6), 909–935.
Devulder, A., Aubry, D., Puel, G., 2010. Two-time scale fatigue modelling: application to damage. Comput. Mech. 45 (6), 637–646.
Doudard, C., Calloch, S., Cugy, P., Galtier, P., Hild, F., 2005. A probabilistic two-scale model for high cycle fatigue life predictions. Fatigue Fract. Eng. Mater. Struct. 28, 279–288.
Eshelby, J., 1957. The determination of the elastic field of an ellipsoidal inclusion, and related problems. Proc. R. Soc. A 241 (1226).
Gaborit, P., 2015. Unification des modèles d'endommagement de type Lemaitre, pour la fatigue LCF/HCF, multiaxiale et aléatoire. Ph.D. thesis. École Normale Supérieure de Cachan.
Gaborit, P., Desmorat, R., Pyre, A., Gilblas, N., 2013. Vers un modèle d'endommagement unifié pour la fatigue à faible et grand nombre de cycles. In: 21ème Congrès Francais de Mécanique.
Gaborit, P., Souto-Lebel, A., Desmorat, R., 2016. Unification de modèles d'endommagement de type lemaitre pour la fatigue à faible et grand nombre de cycles, multiaxiale et aléatoire. In: 35èmes Journées de Printemps de la Société Française de Métallurigue et de Matériaux (SF2M): Fatigue sous chargement d'amplitude variable

et environnement vibratoire.
Giacoma, A., Dureisseix, D., Gravouil, A., Rochette, M., 2015. Toward an optimal a priori reduced basis strategy for frictional contact problems with Latin solver. Comput. Methods Appl. Mech. Eng. 283, 1357–1381.
Gillner, K., Münstermann, S., 2017. Numerically predicted high cycle fatigue properties through representative volume elements of the microstructure. Int. J. Fatigue 105, 219–234.
Glinka, G., 1985. Energy density approach to calculation of inelastic strain-stress near notches and cracks. Eng. Fract. Mech. 22, 405–508.
Haouala, S., Doghri, I., 2015. Modeling and algorithms for two-scale time homogenization of viscoelastic-viscoplastic solids under large numbers of cycles. Int. J. Plast. 70, 98–125.
Heyberger, C., Boucard, P.-A., Néron, D., September 2011. Multiparametric analysis within the proper generalized decomposition framework. Comput. Mech. 49 (3), 277–289.
Kerfriden, P., Gosselet, P., Adhikari, S., Bordas, S.P.-A., 2011. Bridging proper orthogonal decomposition methods and augmented Newton–krylov algorithms: an adaptive model order reduction for highly nonlinear mechanical problems. Comput. Methods Appl. Mech. Eng. 200 (5–8), 850–866.
Kerfriden, P., Passieux, J.-C., Bordas, S.P.-A., 2012. Local/global model order reduction strategy for the simulation of quasi-brittle fracture. Int. J. Numer. Methods Eng. 89 (2), 154–179.
Kröner, E., 1961. Zur plastischen Verformung des Vielkristalls. Acta Metall. 9, 155–161.
Ladevèze, P., 1985a. Tech. Rep.. New Algorithms: Mechanical Framework and Development (In French), vol. 57 LMT-Cachan.
Ladevèze, P., 1985b. On a family of algorithms for structural mechanics (in French). C. R. Acad. Sci. 300 (2), 41–44.
Ladevèze, P., 1999. Nonlinear Computational Structural Mechanics. Mechanical Engineering Series. Springer, New York.
Ladevèze, P., Passieux, J.-C., Néron, D., 2010. The Latin multiscale computational method and the proper generalized decomposition. Comput. Methods Appl. Mech. Eng. 199 (21), 1287–1296.
Ladevèze, P., Lemaitre, J., 1984. Damage effective stress in quasi-unilateral conditions. In: 16th International Congress of Theoretical and Applied Mechanics.
Lautrou, N., Thevenet, D., Cognard, J.-Y., 2009. Fatigue crack initiation life estimation in a steel welded joint by the use of a two-scale damage model. Fatigue Fract. Eng. Mater. Struct. 32 (5), 403–417.
Lemaitre, J., 1996. A Course on Damage Mechanics. Springer, Berlin.
Lemaitre, J., Desmorat, R., 2005. Engineering Damage Mechanics: Ductile, Creep, Fatigue and Brittle Failures. Springer.
Lemaitre, J., Doghri, I., 1994a. Damage 90: a post processor for crack initiation. Comput. Methods Appl. Eng. 115, 197–232.
Lemaitre, J., Doghri, I., 1994b. Damage 90: a post-processor for crack initiation. Comput. Methods Appl. Mech. Eng. 115, 197–232.
Lemaitre, J., Sermage, J., Desmorat, R., 1999. A two scale damage concept applied to fatigue. Int. J. Fract. 97 (1–4), 67–81.
Monchiet, V., Charkaluk, E., Kondo, D., 2006. Plasticity-damage based micromechanical modelling in high cycle fatigue. Compt. Rendus Mec. 334 (2), 129–136.
Néron, D., Boucard, P.-A., Relun, N., 2015. Time-space pgd for the rapid solution of 3d nonlinear parametrized problems in the many-query context. Int. J. Numer. Methods Eng. 103 (4), 275–292.
Neuber, H., 1961. Theory of stress concentration for shear-strained prismatical bodies with arbitrary nonlinear stress-strain law. J. Appl. Mech. 28 (4), 544–550.
Ottosen, N.S., Stenström, R., Ristinmaa, M., 2008. Continuum approach to high-cycle fatigue modeling. Int. J. Fatigue 30 (6), 996–1006.
Relun, N., Néron, D., Boucard, P.-A., 2011. Multiscale elastic-viscoplastic computational analysis. Eur. J. Comput. Mech. 20 (7–8), 379–409.
Relun, N., Néron, D., Boucard, P.-A., 2013. A model reduction technique based on the PGD for elastic-viscoplastic computational analysis. Comput. Mech. 51, 83–92.
Ryckelynck, D., Missoum Benziane, D., Cartel, S., Besson, J., 2011. A robust adaptive model reduction method for damage simulations. Comput. Mater. Sci. 50, 1597–1605.
Tang, J., Hu, W., Meng, Q., Sun, L., Zhan, Z., 2017. A novel two-scale damage model for fatigue damage analysis of transition region between high- and low-cycle fatigue. Int. J. Fatigue 105, 208–218.
Van Paepegem, W., Degrieck, J., De Baets, P., 2001. Finite element approach for modelling fatigue damage in fibre-reinforced composite materials. Compos. Part B 32, 575–588.
Xiao, Y.-C., Li, S., Gao, Z., 1998. A continuum damage mechanics model for high cycle fatigue. Int. J. Fatigue 20 (7), 503–508.
Zaoui, A., 1985. Homogenization Techniques for Composite Media. Lecture Notes in Physics. Springer (Ch. Approximate statistical modelling and applications).